


Cite this: *RSC Adv.*, 2022, 12, 18685

# Reinforcement of nanoporous lanthanum-doped zinc borate by vanadium selenide nanosheets for improved tribological activity†

Alok K. Singh,<sup>a</sup> Nivedita Shukla,<sup>a</sup> Kavita,<sup>a</sup> Dinesh K. Verma,<sup>b</sup> Bharat Kumar,<sup>c</sup> K. D. Mandal<sup>ID</sup><sup>a</sup> and Rashmi B. Rastogi<sup>ID</sup><sup>\*a</sup>

Nanoporous zinc borate (ZB) and 10% lanthanum-doped porous zinc borate (LZB) were synthesized to explore the role of porosity and doping in zinc borate during lubrication. HR-SEM, TEM, and HR-TEM authenticated nanoporous structures. The tribological properties of their blends with paraffin oil (PO) were compared by employing ASTM D4172 and ASTM D5183 norms on a four-ball tester. Vanadium selenide nanosheets (VSe<sub>2</sub>) were used to reinforce the structure of LZB for further advancement of the tribological properties. The superiority of the LZB/VSe<sub>2</sub> over LZB and VSe<sub>2</sub> nanosheets could be adjudged by tribological data. The porosity and lanthanum doping have yielded commendable tribological activity. The VSe<sub>2</sub> nanosheets have strengthened the LZB matrix. The other constituent oxides of tribofilm from the LZB matrix, based on EDX analysis and XPS studies of the worn surface, ZnO, B<sub>2</sub>O<sub>3</sub>, La<sub>2</sub>O<sub>3</sub>, and V<sub>2</sub>O<sub>5</sub>, have abetted lubrication. The AFM and SEM investigations of wear track corroborated the tribological results.

Received 3rd May 2022  
Accepted 14th June 2022

DOI: 10.1039/d2ra02806a

rsc.li/rsc-advances

## 1 Introduction

Two-dimensional layered nanomaterials, like graphene, graphitic carbon nitride, molybdenum disulfide, tungsten disulfide, and metal-organic frameworks, have numerous research applications because of a large specific surface area and weak physical interactions (van der Waals type) existing amongst the adjacent layers.<sup>1–4</sup> These weak interactions furnish outstanding thermal, mechanical, optical, and electrical properties to such nanomaterials.<sup>1</sup> Consequently, their applications have been fully admitted in diverse fields, like catalysis, sensors, photonics, water splitting, energy-storing, hydrogen evolution, and electronics.<sup>1</sup>

Furthermore, for the sustainability of the machine and durability of its components, 2D nanomaterials have been frequently used as wear and friction-reducing additives to the base lubricating oil.<sup>1–3,5,6</sup> Recently, the tribological properties of some metal selenides such as MoSe<sub>2</sub>, WSe<sub>2</sub>, NbSe<sub>2</sub>, and monoselenide ZnSe, have been investigated.<sup>7–12</sup> Zhao *et al.* investigated macroscale superlubricity of MoS<sub>2</sub>/MoSe<sub>2</sub>

heterostructures.<sup>13</sup> The lubricating properties of MoS<sub>2</sub> and WSe<sub>2</sub>-based nanocomposite coatings were studied by Meister and coworkers.<sup>14</sup> Zhang and associates studied the tribological behavior of ZnSe nanoplates as lubricant additives.<sup>12</sup> The lubricating behavior of MoSe<sub>2</sub> hollow nanospheres, nano-flowers, and MoSe<sub>2</sub> hybrids with other nanomaterials was studied in detail.<sup>15–17</sup> Zhang and collaborators have shown the tribological applications of the composite of a copper matrix reinforced with Ni/NbSe<sub>2</sub>.<sup>18</sup> Ultrasound-assisted preparation of NbSe<sub>2</sub> micro/nanoparticles and hybrid material was achieved by Qu and coworkers.<sup>10</sup> They tested them for sliding electrical contact as a solid lubricant. The tribological properties of hexagonal NbSe<sub>2</sub> nanoplates were examined by Sun *et al.*<sup>19</sup> Cao and his associates studied the tribological behavior of the tower-like structure of WSe<sub>2</sub> ultrathin nanosheets as an additive to paraffin oil.<sup>9</sup> Besides the above selenides, VSe<sub>2</sub> also holds a layered hexagonal lamellar structure and is well known mainly for hydrogen evolution reactions.<sup>20,21</sup> Li and coworkers tested VSe<sub>2</sub> nanosheets for ultrafast fiber lasers.<sup>22</sup> Investigations on VSe<sub>2</sub> nanosheets for the storage of alkali metal ions were conducted by Ming *et al.*<sup>23</sup> and Yang *et al.*<sup>24</sup> The nanocomposite of VSe<sub>2</sub> with graphene was used as anode for Li-ion batteries by Wang *et al.*<sup>25</sup> and as cathode material for an aqueous zinc-ion battery by Narayanasamy *et al.*<sup>26</sup> Ghobadi and associates<sup>27</sup> investigated the catalytic properties of VSe<sub>2</sub>. NbSe<sub>2</sub>, VSe<sub>2</sub> being congeners, VSe<sub>2</sub> is expected to be a potential lubricant additive like NbSe<sub>2</sub>; however, to the best of our knowledge, the tribological properties of VSe<sub>2</sub> have not been explored.

<sup>a</sup>Department of Chemistry, Indian Institute of Technology (Banaras Hindu University), Varanasi-221005, India. E-mail: rashmi.apc@iitbhu.ac.in

<sup>b</sup>Department of Chemistry, Prof. Rajendra Singh (Rajju Bhaiya) Institute of Physical Sciences for Study & Research, V.B.S. Purvanchal University, Jaunpur-222003, U.P., India

<sup>c</sup>Intellectual Property Office Mumbai, 400037, the government of India

† Electronic supplementary information (ESI) available. See <https://doi.org/10.1039/d2ra02806a>


On the other hand, boron-containing compounds in general metal borates, particularly calcium borate,<sup>28</sup> lanthanum borate,<sup>29</sup> and zinc borate are known for their outstanding lubrication behavior. Zinc borate has explicitly been found to be used as an additive to reduce friction and wear. Tian and associates studied the coefficient of friction of nanodisc zinc borate and zinc borate core-shell with SiO<sub>2</sub> nanosphere.<sup>30,31</sup> Zhao and his group exhibited only 14% and 10% reduction in coefficient of friction and wear scar diameter, respectively, using 0.5% zinc borate ultrafine powder in sunflower oil employing a pin-on-disc tribotester.<sup>32</sup> They also investigated lubricating properties of the same without and with surface modification in liquid paraffin oil. They found that wear scar diameter (WSD) increases with zinc borate powder compared to base oil alone; however, WSD decreases after surface modification.<sup>33</sup> The tribological investigations of chemically capped nanocomposites of zinc borate with MoS<sub>2</sub> (ZB/MoS<sub>2</sub>) and graphene oxide (2.0 wt% of ZB/GO) were achieved by Wu *et al.*<sup>34</sup> and Cheng *et al.*,<sup>35</sup> respectively. It was noted that the friction coefficient of ZB/GO reduced remarkably compared to ZB/MoS<sub>2</sub>, while the opposite trend was observed for wear reduction. Dong and coworkers studied the friction-reducing and antiwear properties of the nano zinc borate with dispersing agent sorbitol monostearate in paraffin oil. They observed an almost 50% drop in coefficient of friction and 10% in WSD.<sup>36</sup>

Further, it has been reported that the tribological functioning under a ravenous condition can be enhanced by improving the lubricating oil-storage capability of the system.<sup>37,38</sup> In the case of porous G-Ni composite, it has been noted that the porosity adds to lubrication behavior in oil.<sup>39</sup> Xiao *et al.* have observed improved mechanical and tribological properties of porous metallic cubic boron nitride reinforced with graphene nanoparticles.<sup>40</sup> The lubrication properties of porous alumina ceramic matrix have been significantly facilitated by immersing polymethyl methacrylate (PMMA)/poly alpha olefins (PAO6) microcapsules.<sup>41</sup>

Additionally, the mechanical property of zinc borate glass has been improved by lanthanum doping.<sup>42</sup> It has been reported that varying concentrations of lanthanum doping have triggered the dosimetric character and thermo-luminescence of zinc borates.<sup>43,44</sup> The enhancement in tribological properties of doped nanomaterials, like magnesium doped zinc oxide, ceria doped zirconia, lanthanum-doped yttria, has been reported from our laboratory.<sup>1,5,45</sup> Furthermore, the composites of the doped nanomaterials with layered materials like graphene, graphitic carbon nitride, molybdenum disulfide, and copper phthalocyanine have been proclaimed from our group to manifest exemplary tribological behavior.<sup>1,3,5,6</sup>

Considering the above, it engrossed us to synthesize nanoporous zinc borate (ZB), lanthanum doped zinc borate (LZB), lamellar vanadium selenide (VSe<sub>2</sub>), and use the synthesized VSe<sub>2</sub> to reinforce LZB (LZB/VSe<sub>2</sub>) for upgrading its tribological behavior. Accordingly, VSe<sub>2</sub> nano-sheets, ZB, LZB, and LZB/VSe<sub>2</sub> were synthesized, and their tribological activity was appraised in paraffin oil (PO) on a four-ball tester machine under ASTM D4172 and ASTM D5183 conditions.

## 2 Experimental section

### 2.1. Materials

Analytical Reagent grade chemicals from Merck India have been used throughout the current work.

### 2.2. Preparation of additives

**2.2.1. Preparation of nanoporous zinc borate and La-doped zinc borate.** The syntheses of zinc borate and 10% lanthanum-doped zinc borate were brought about by the auto combustion route. For the preparation of zinc borate, Zn(NO<sub>3</sub>)<sub>3</sub>·6H<sub>2</sub>O (4.1 g), citric acid (3.184 g), and borax (5.08 g) were mixed in distilled water (100 mL) in a beaker and heated at nearly 210 °C with continuous stirring until a gel was produced that turned into black powder. Black powder was calcined at 500 °C for 3 h in a muffle furnace, producing zinc borate. Lanthanum-doped (10%) zinc borate was prepared in the same way using La(NO<sub>3</sub>)<sub>3</sub>·6H<sub>2</sub>O (0.367 g), Zn(NO<sub>3</sub>)<sub>3</sub>·6H<sub>2</sub>O (2.34 g), borax (3.32 g), and citric acid (2.0 g).

**2.2.2. Preparation of VSe<sub>2</sub> nanosheets.** VSe<sub>2</sub> nanosheets were prepared hydrothermally.<sup>46</sup> 10 mmol SeO<sub>2</sub> (2.22 g), 5 mmol NH<sub>4</sub>VO<sub>3</sub> (1.17 g), and 150 mL distilled water were mixed and stirred for 15 min followed by dropwise addition of 25 mL HCOOH with continuous stirring for 10 min. The contents were shifted into a Teflon autoclave of 200 mL capacity and kept in an oven at 200 °C for 24 h. The collected mixture was cooled down to ambient temperature, filtered and washed through ethanol and deionized water 5–7 times, and then dried at 70 °C to get bulk VSe<sub>2</sub> powder. The bulk VSe<sub>2</sub> powder was exfoliated by ultrasonication for 2 to 3 h in a 50% alcohol-water mixture (200 mL). The dispersion was centrifugated for 20 min at 3500 rpm. The solvent of the supernatant was evaporated to obtain the VSe<sub>2</sub> nanosheets.

**2.2.3. Preparation of VSe<sub>2</sub> reinforced porous La-doped zinc borate.** Vse<sub>2</sub> nanosheets (600 mg) and LZB (400 mg) were taken individually in ethanol (50 mL) and ultrasonicated for 15 min at around 40 °C. The obtained dispersions were mixed and refluxed at 80 °C for 24 h. The resultant colloidal dispersion was filtered and dried at 60 °C. Finally, a grayish-black La-doped zinc borate/lamellar VSe<sub>2</sub> was obtained.

A schematic representation for LZB/VSe<sub>2</sub> synthesis is given in Scheme 1.

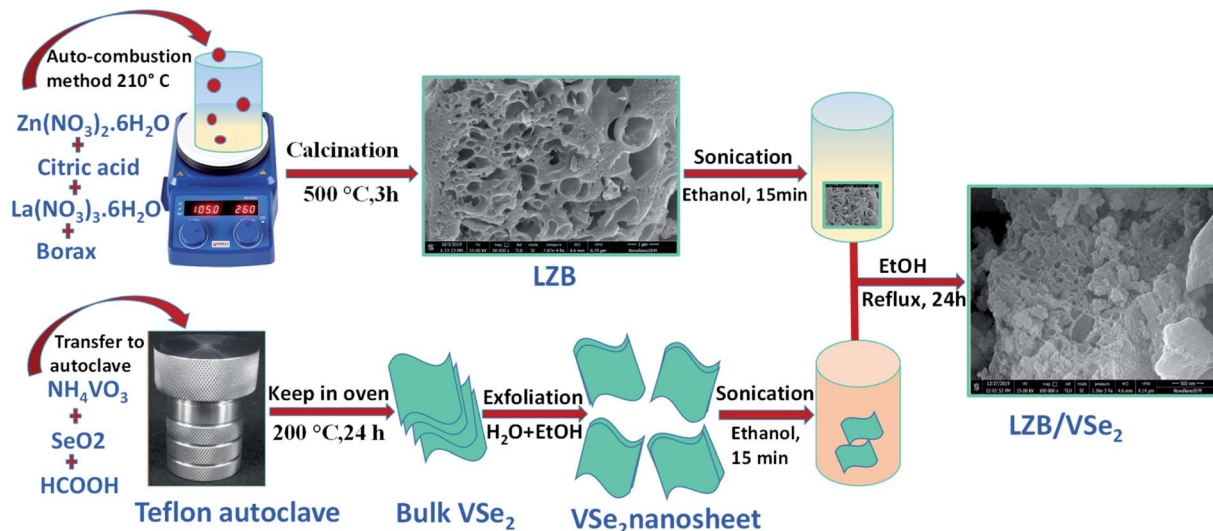
### 2.3. Characterization of additives

The characterization of the synthesized nanomaterials was accomplished by XRD, FTIR, XPS, HR-SEM, EDX, and TEM/HR-TEM. The instruments utilized are elaborated in ESI, ESI-1.1†.

### 2.4. Tribological test

The Physico-chemical characteristics of PO are provided in ESI-1.2. Test samples were prepared *via* 1 h sonication for different concentrations of the synthesized additives; 0.00, 0.10, 0.15, 0.20, and 0.25% w/v, in PO at room temperature. From ASTM D4172 and ASTM D5183 test standards, the wear and friction reducing properties and load-carrying capacity were obtained,



Scheme 1 Schematic presentation of synthesis of LZB/VSe<sub>2</sub>.

respectively. The details of the experiments have been described in ESI-1.2, and tribological parameters are provided in ESI-1.3. The characterization of the worn surface conducted by SEM, AFM, and XPS has been narrated in ESI-1.4.

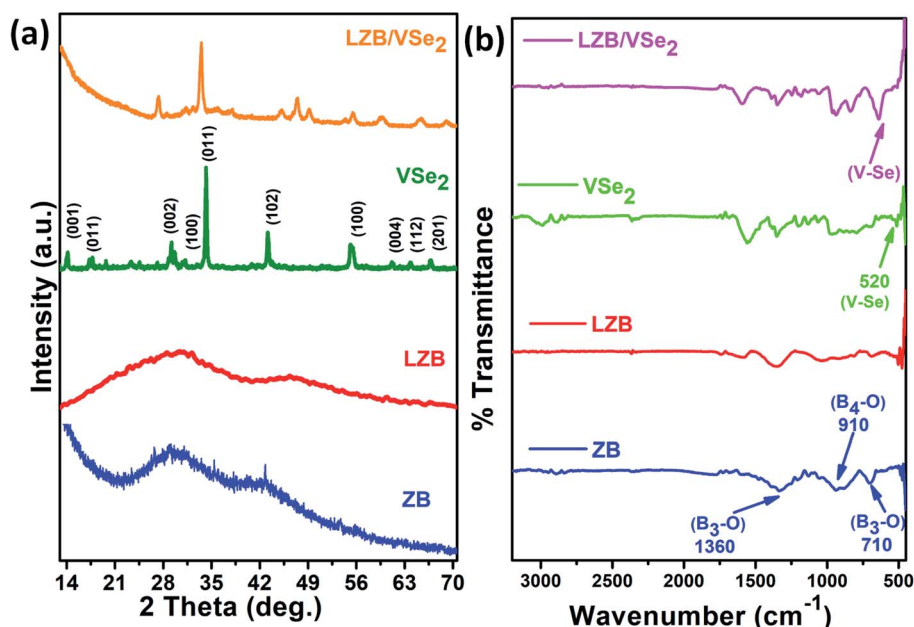
### 3 Results and discussion

#### 3.1. Morphological investigation of ZB, LZB, VSe<sub>2</sub>, and the LZB/VSe<sub>2</sub>

The synthesized additives were studied using XRD, FT-IR, SEM/HR-SEM, TEM/HR-TEM UV/visible, and XPS. Fig. 1a reveals XRD patterns of VSe<sub>2</sub>, ZB, LZB and LZB/VSe<sub>2</sub>. Well-defined diffraction peaks are obtained for VSe<sub>2</sub> nanosheets and assigned to

hexagonal structure (JCPDS no. 89–1641).<sup>23</sup> In the diffraction pattern of ZB and LZB, a broad peak at 29.5° is identified for their amorphous structure.<sup>34,35</sup> The heterostructure LZB/VSe<sub>2</sub> did not exhibit any new peaks except those of VSe<sub>2</sub> and LZB. It signifies that VSe<sub>2</sub> nanosheets have efficaciously physically adhered to the surface of LZB, but the intensity of the peaks is considerably reduced.

Fig. 1b illustrates the IR spectra of the additives. The IR spectrum of ZB shows asymmetric stretching frequencies ( $\nu_{\text{as}}$ ) of four and three-coordinate boron at 910 cm<sup>-1</sup> and 1360 cm<sup>-1</sup>, respectively, while the symmetric stretching mode ( $\nu_{\text{s}}$ ) of three-coordinate boron is visible at 710 cm<sup>-1</sup>.<sup>47</sup> However, in the spectrum of LZB, the  $\nu_{\text{as}}$  for four coordinate boron is shifted

Fig. 1 (a) XRD patterns of ZB, LZB, VSe<sub>2</sub>, and LZB/VSe<sub>2</sub> (b) IR of ZB, LZB, VSe<sub>2</sub>, and LZB/VSe<sub>2</sub>.



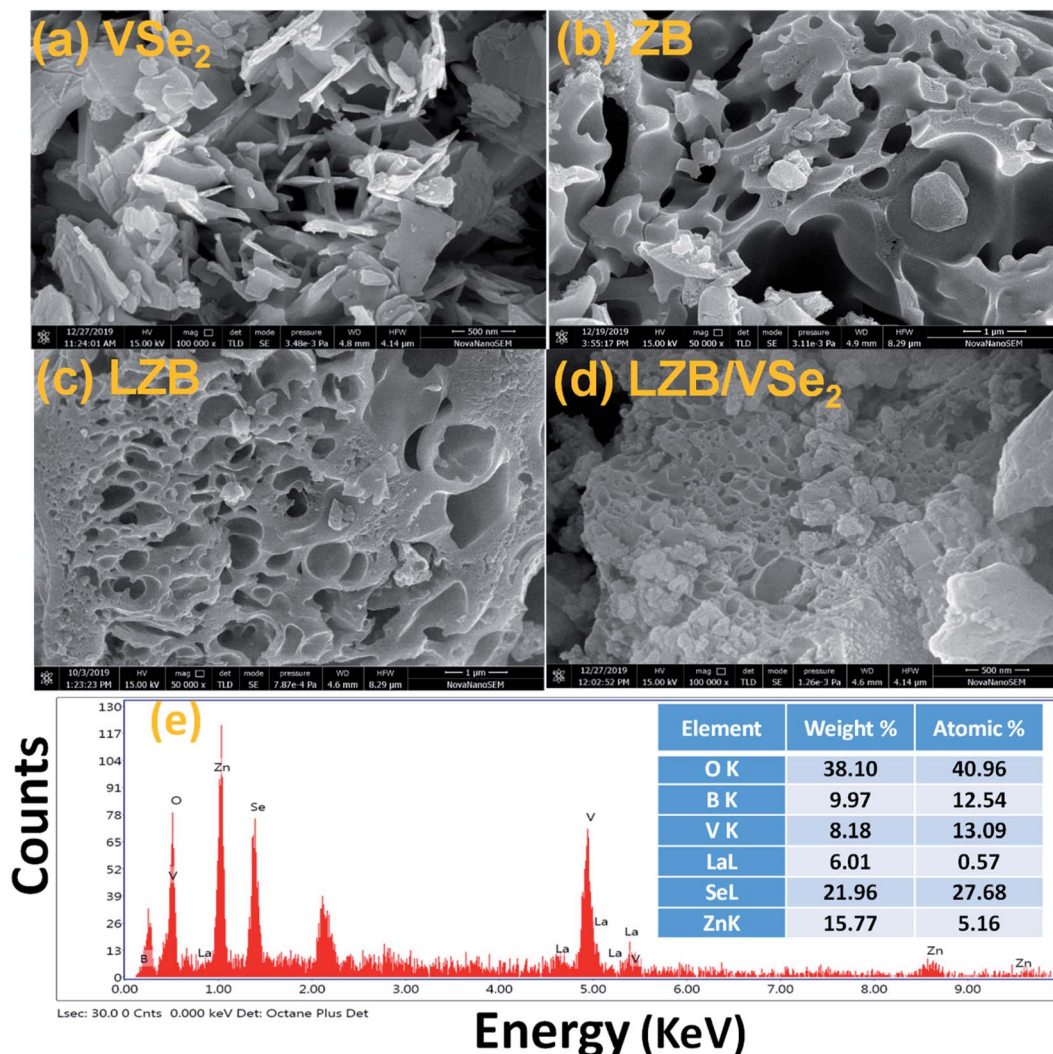


Fig. 2 HR-SEM images of (a)  $\text{VSe}_2$ , (b) ZB, (c) LZB, (d) LZB/ $\text{VSe}_2$  and (e) EDX spectrum of LZB/ $\text{VSe}_2$ .

positively to around  $1050\text{ cm}^{-1}$ . The spectrum of  $\text{VSe}_2$  is characterized by a peak at  $520\text{ cm}^{-1}$  due to  $\nu$  V-Se, which is identified at approximately  $630\text{ cm}^{-1}$  in the LZB/ $\text{VSe}_2$ .<sup>48</sup> The blue shift of the peak is attributed to the significant interaction of  $\text{VSe}_2$  with the LZB.

The HR-SEM images of ZB, LZB,  $\text{VSe}_2$ , and LZB/ $\text{VSe}_2$  were recorded to inspect their morphologies, Fig. 2a–d, respectively. Fig. 2a and b discern irregular mesoporous and macroporous structures for ZB and LZB with pores of enormously varying size (4 nm to 500 nm) well-scattered throughout. Randomly assembled fluffy nanosheets of  $\text{VSe}_2$  are observable in Fig. 2c. The lateral measurement of nanosheets lies in the range 100 nm to 700 nm with a thickness of 10–70 nm as calculated by Image J software. Fig. 2d reveals  $\text{VSe}_2$  nanosheets spread over and into the pores of La-doped ZB heterostructure depending upon the pore diameter of LZB. The EDX analysis of the LZB/ $\text{VSe}_2$ , Fig. 2e, confirms the constituent elements zinc, vanadium, lanthanum, selenium, boron, and oxygen, endorsing the interaction between LZB and  $\text{VSe}_2$ . EDX spectra of ZB, LZB, and  $\text{VSe}_2$  have been given in ESI (Fig. S1)†.

For a more distinct discernment of the morphology, TEM images of vanadium selenide, ZB, LZB, and LZB/ $\text{VSe}_2$  have also been documented and are presented in Fig. 3a–d, respectively. In Fig. 3a, the lamellar structure of  $\text{VSe}_2$  is prominently visible with the lattice fringes as 0.26 nm corresponding to the (011) plane.<sup>49</sup> The mesoporous and microporous structures of ZB and LZB can be clearly observed in Fig. 3b and c. The amorphous nature of ZB and LZB can be seen from the selected area diffraction (SAED) pattern, as shown in the inset of the corresponding figure. Fig. 3d delineates the anchored  $\text{VSe}_2$  nanosheets on porous LZB. The interlayer distance of the  $\text{VSe}_2$  nanosheets related to the (011) plane has increased to 0.28 nm in the reinforced structure, as observed in its HR-TEM (Fig. 3d<sub>1</sub>). The increase of the interlayer distance of the (011) plane in  $\text{VSe}_2$  nanosheets emphasizes their interaction with the La-doped ZB. The SAED pattern of the reinforced structure, shown in the inset, reveals substantial crystallinity.

The XPS studies could establish the chemical states of the elements in the LZB/ $\text{VSe}_2$ . The deconvoluted core level spectra of La 3d, Zn 2p, B 1s, O 1s, V 2p, and Se 3d are shown in Fig. 4



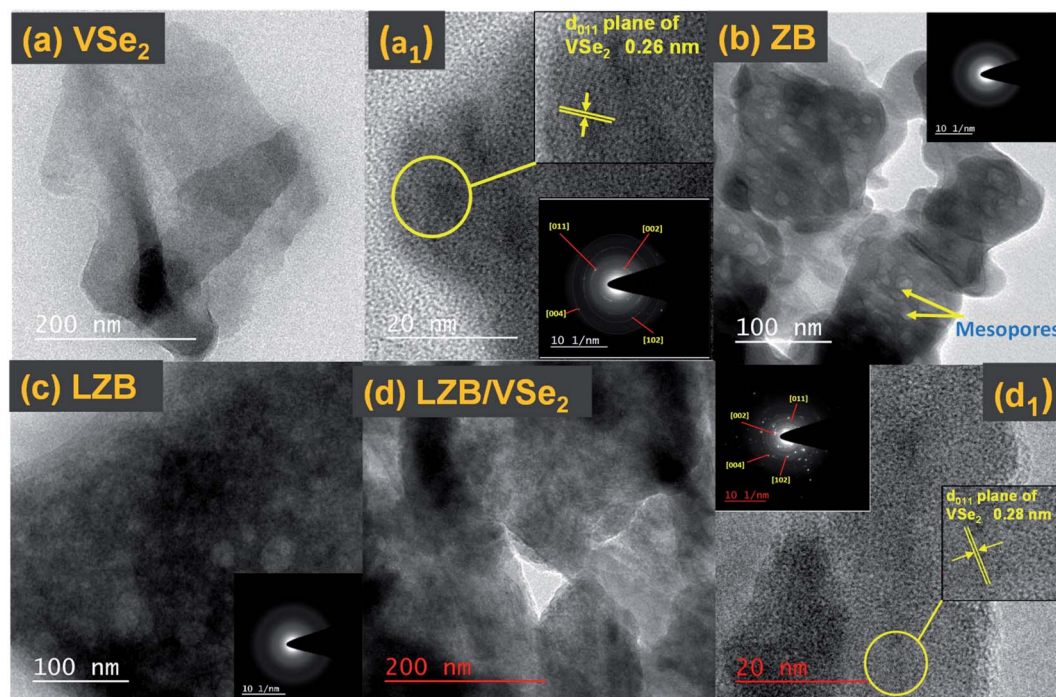


Fig. 3 TEM photograph of (a)  $\text{VSe}_2$ , (b) ZB, (c) LZB, (d) LZB/ $\text{VSe}_2$  and HR-TEM pictures of  $\text{VSe}_2$  ( $a_1$ ) and LZB/ $\text{VSe}_2$  ( $d_1$ ). The insets in (Fig.  $a_1$  and  $d_1$ ) display the SAED patterns of the additives.

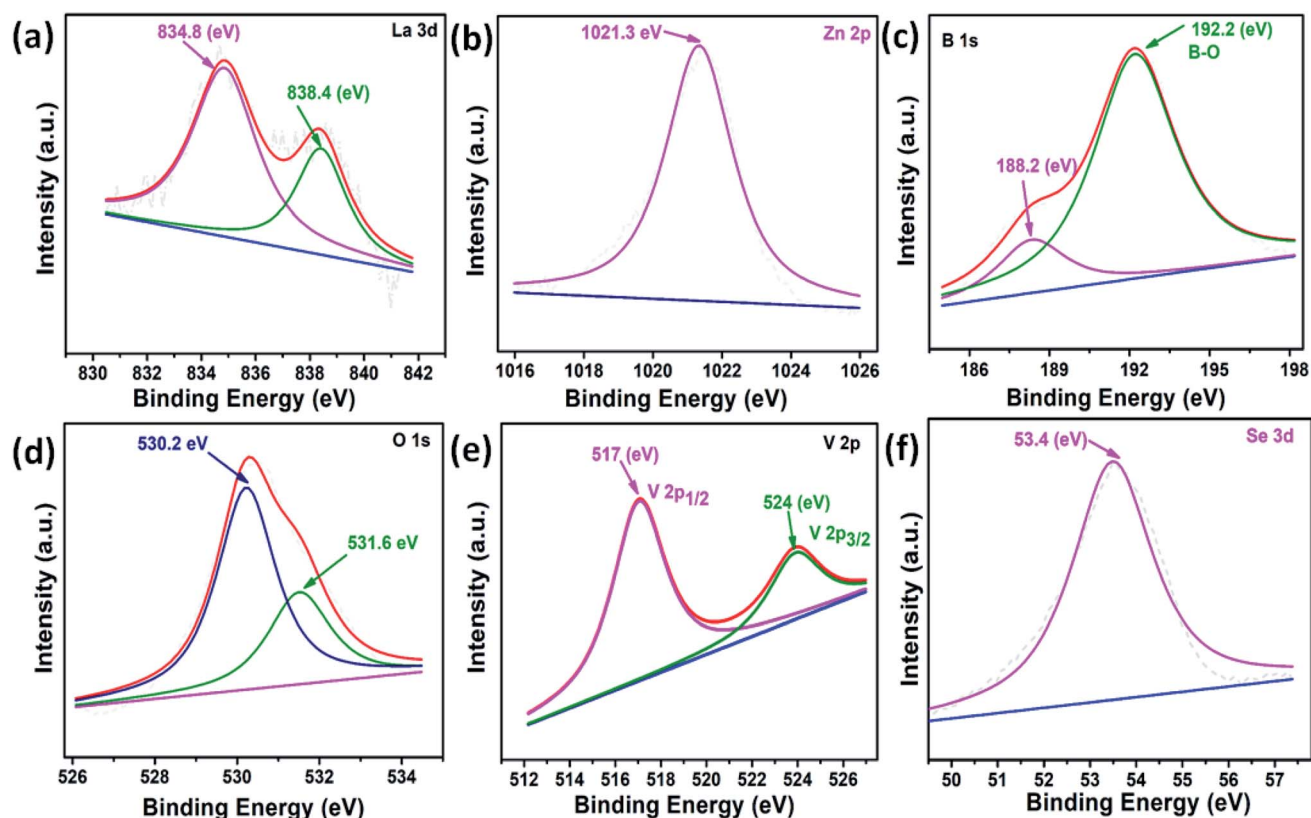


Fig. 4 Deconvoluted core-level XPS spectra of (a) La 3d, (b) Zn 2p, (c) B 1s, (d) O 1s (e) V 2p and (f) Se 3d.



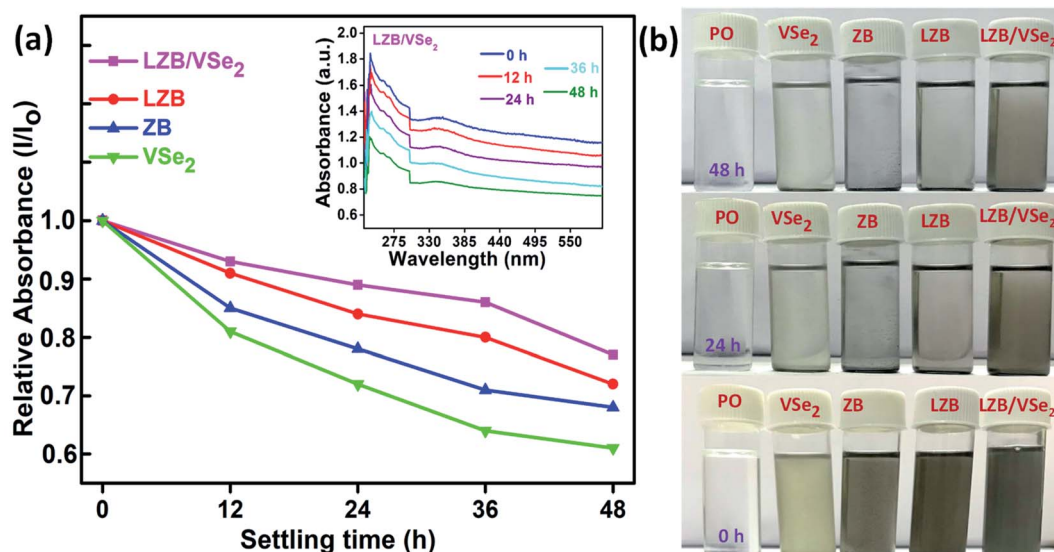


Fig. 5 (a) Dispersion stabilities of base lube comprising  $VSe_2$ , ZB, LZB, and LZB/ $VSe_2$  by UV-vis spectrophotometry, (b) Visual snapshots of the admixtures dispersed in base lube at 0, 24, and 48 h.

using peak fit software. The core-level spectrum of La 3d reveals peaks at binding energies 834.8 and 838.8 eV conforming to the  $La^{3+}$ , Fig. 4a.<sup>5</sup> The presence of a peak at binding energy

1021.3 eV in the Zn 2p spectrum, Fig. 4b, corresponds to Zn  $2p_{1/2}$  (Zn–O bond).<sup>3,50,51</sup> Fig. 4c displays two peaks at 188.2 eV and 192.2 eV, indicating the boron oxygen bond.<sup>50,51</sup> The O 1s

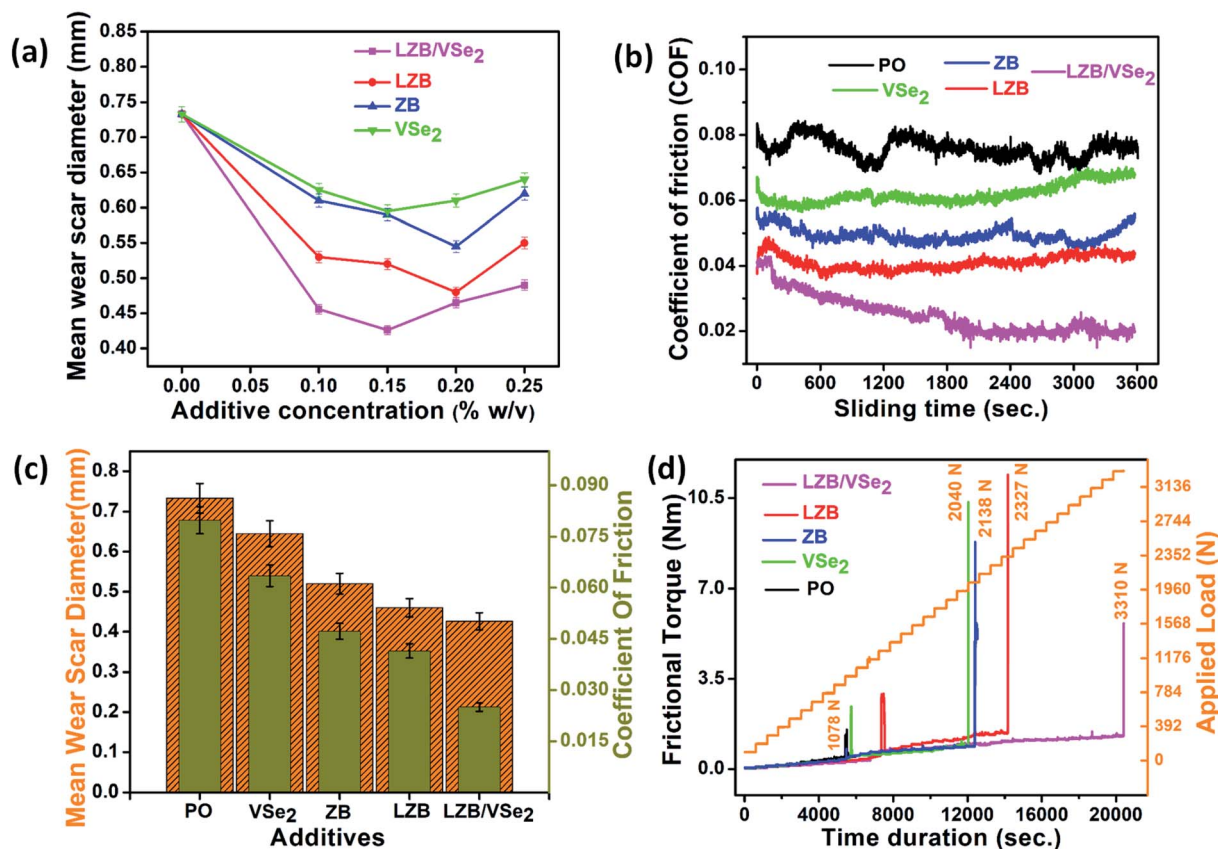


Fig. 6 (a) ASTM D4172 test results to optimize the concentration of different additives (b) COF against sliding time (c) average coefficient of friction and the MWD in the format of bar diagram (d) frictional torque vs. load and time for plain PO and with different additives under ASTM D5183 standards.



**Table 1** Cutbacks in frictional power for individual additives in PO at the optimized concentration, 0.15% (w/v)

	Additives	Power consumption (MJ)	Reduction in power consumption	% Reduction in power consumption
1	PO	0.0628	–	–
2	VSe <sub>2</sub>	0.0590	0.0038	6.00
3	ZB	0.0375	0.0253	40.30
4	LZB	0.0330	0.0298	47.45
5	LZB/VSe <sub>2</sub>	0.0190	0.0438	69.74

spectrum, Fig. 4d, exhibits peaks at 530.2 and 531.6 eV for metal oxides bonds [La–O and Zn–O] and absorbed water, respectively.<sup>3,5</sup> In the core-level V 2p spectrum, the peaks appearing at

binding energies 517 eV (V 2P<sub>1/2</sub>) and 524 eV (V 2P<sub>3/2</sub>), Fig. 4e, indicate the occurrence of V<sup>4+</sup> ions.<sup>24</sup> The peak at 53.4 eV corresponds to Se<sup>2–</sup><sub>20,23</sub> in Fig. 4f.

### 3.2. Tribological behavior of the additives

**3.2.1. Dispersion stability of additives in base lube.** For tribological applications, the dispersion stability of the nano-fluids is of particular concern. Electronic spectroscopy (UV/visible) has been helpful for the said objective. The additives (optimized concentration) were ultrasonicated in the base lube and then diluted 10 times. The absorbance data of dilute dispersions were noted down starting from 0 to 48 h. Fig. 5a displays the plot of relative absorbance of the dispersions *versus* settling time. The magnitude of reduction in relative absorbance with time relates to the stability of the dispersion.

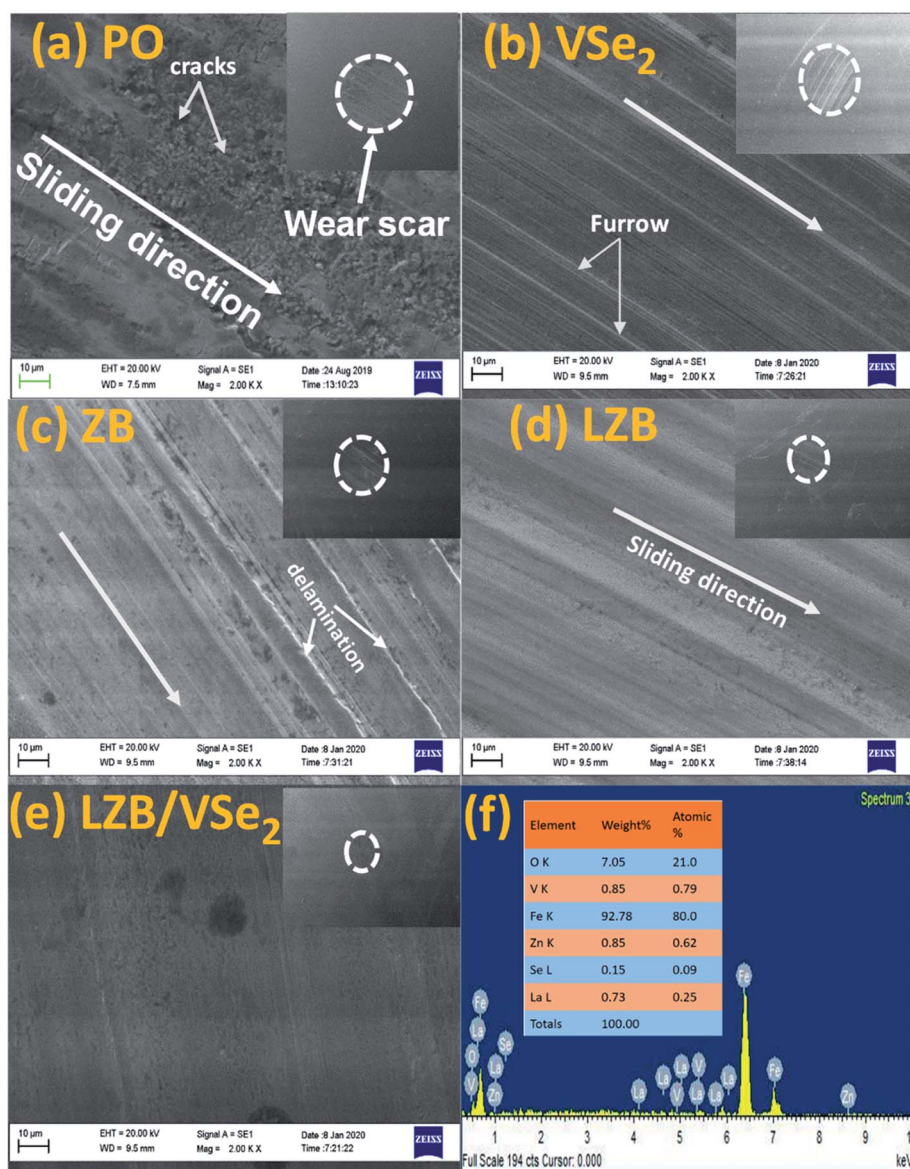


**Fig. 7** (a)–(e) SEM micrographs of the worn surfaces in the presence of PO with and without additives (0.15% w/v) at 2.00 K X amplification under the ASTM D4172 conditions, inset displaying wear scar surface at higher amplification 100 K X (f) EDX spectrum of wear track of steel surface lubricated with LZB/VSe<sub>2</sub>.





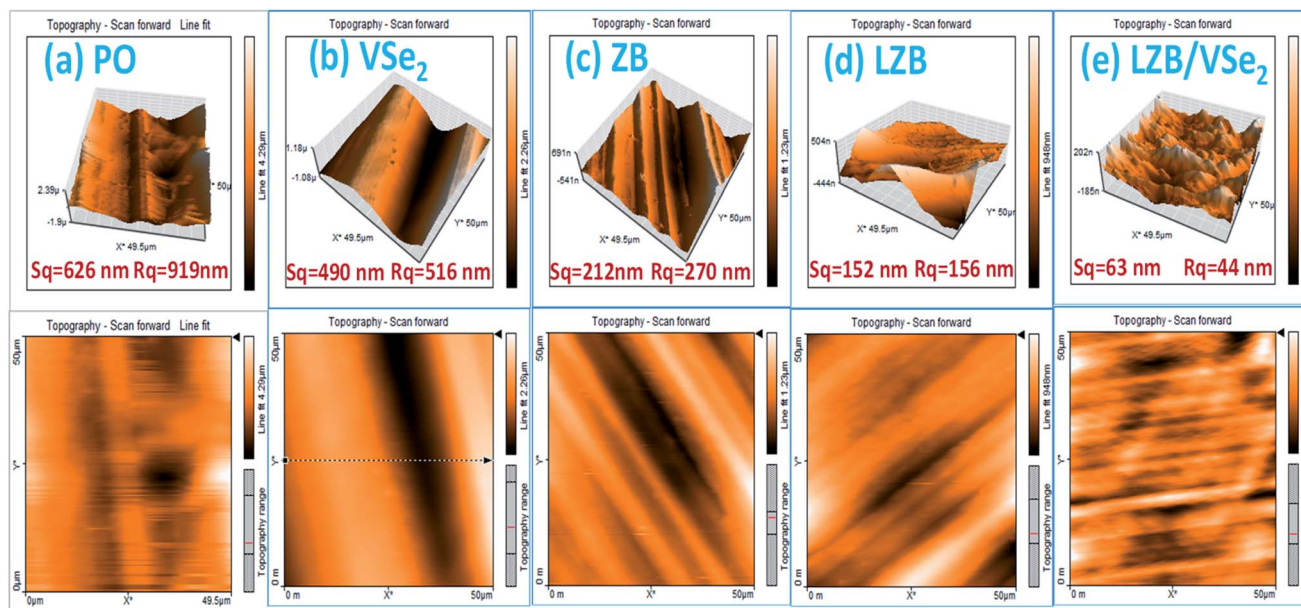


Fig. 8 3D and 2D AFM images of the wear track lubricated with optimized concentration of blends of additives in PO after conducting ASTM D4172 test, (a) PO, (b) VSe<sub>2</sub>, (c) ZB (d) LZB, and (e) LZB/VSe<sub>2</sub>.

Apparently, the reinforced structure attains maximum dispersion stability, followed by LZB, ZB, and at last VSe<sub>2</sub>.

In the inset of Fig. 5a, the absorbance values of the LZB/VSe<sub>2</sub> in the beginning and after 12, 24, 36 and 48 h are displayed at approximately 230 nm. Fig. 5b presents snapshots of the base lube and the dispersions in the beginning, after 24 and 48 h.

**3.2.2. Concentration optimization.** For describing the efficacy of the additives, the concentration is a vital variant; it must be optimized first. For this, ASTM D4172 standard test (392 N applied load for 60 min at 1200 rpm) was performed in PO with the admixtures in different concentrations, 0.0, 0.10, 0.15, 0.20, and 0.25% w/v and their corresponding mean wear scar diameter (MWD) were noted. A plot of MWD vs. concentration of the additives was drawn, as depicted in Fig. 6a. Compared to base lube, values decrease significantly for all the analyzed concentrations of all the additives. Accordingly, wear-reducing behavior is evident at the tested concentrations for all the test materials, but the antiwear efficacies vary extensively. In the case of plain base lube, MWD was noted as 0.735 mm. The relative performance of all additives was found better than the base lube. In general, the MWD reduced up to 0.20% w/v, but beyond that, it rises, excluding the LZB/VSe<sub>2</sub> where MWD rises after 0.15% w/v. Thus, 0.15% of w/v has been taken as the optimized concentration for performing the tests. Variation of MWD in descending order VSe<sub>2</sub> (0.61 mm), ZB (0.545 mm), LZB (0.48 mm), and LZB/VSe<sub>2</sub> (0.426 mm) proves the superiority of the reinforced structure over others.

The optimization of COF vs. additive concentration for each additive is demonstrated in ESI (Fig. S2†), showing the minimum antifriction behavior for VSe<sub>2</sub> at (0.15% w/v), ZB (0.2% w/v), LZB (0.2% w/v) and for LZB/VSe<sub>2</sub> (0.15% w/v). Fig. 6b shows the deviation of coefficient of friction (COF) of the PO alone and its blends with additives vs. time at an optimized

concentration of 0.15% w/v. COF is generally relatively greater in each case at the initial stages due to the lack of tribofilm. With the increase of operating time, the COF becomes stable based on *in situ* formed tribofilm. Irregular behavior of COF in the absence of additive has been articulated in the figure; however, COF is almost uniform when the additives are used. The nature of tribofilm precisely related to the smoothness of the plot. Thus, it is evident that in the case of LZB/VSe<sub>2</sub>, tribofilm formed is adherent, homogeneous, and stable.

**3.2.3. Antiwear and anti-friction properties.** The ASTM D4172 test was conducted for plain PO and its admixtures with different additives to assess antiwear properties. The outcome of the trial is displayed in Fig. 6c in the format of a bar diagram wherein both the COF and MWD have been demonstrated conjunctly. It is clear from the graph that the MWD value for PO alone, 0.735 mm, has dropped in each case, showing a % reduction with VSe<sub>2</sub> (18%), ZB (25.86%), LZB (35%), and while LZB/VSe<sub>2</sub> (43%). The drop in MWD is indicative of antiwear efficacy. There is a 9.14% reduction in MWD ongoing from ZB to LZB; thus, La-doping in ZB has improved the activity. The reinforced structure is better efficacious than LZB, while LZB is superior to ZB and VSe<sub>2</sub>. The % decrease in average COF value of base lube, 0.079, follows the same pattern as that of MWD; VSe<sub>2</sub> (13%), ZB (41%), LZB (49%), and the LZB/VSe<sub>2</sub> (69%).

**3.2.4. Load-carrying ability.** At first, the ASTM D5183 test was performed for the optimized concentration of the additives under the following experimental conditions; 392 N load, 600 rpm, temperature 75 °C, and 60 min to complete the running-in period. After that, the steady-state test is followed by a successive increment of 98 N load at each 10 min cycle until the accomplishment of seizure load due to immediate upsurge of frictional torque, as shown in Fig. 6d. In the case of base lube, a seizure occurs at the load 1078 N. Subsequently, the adjacent





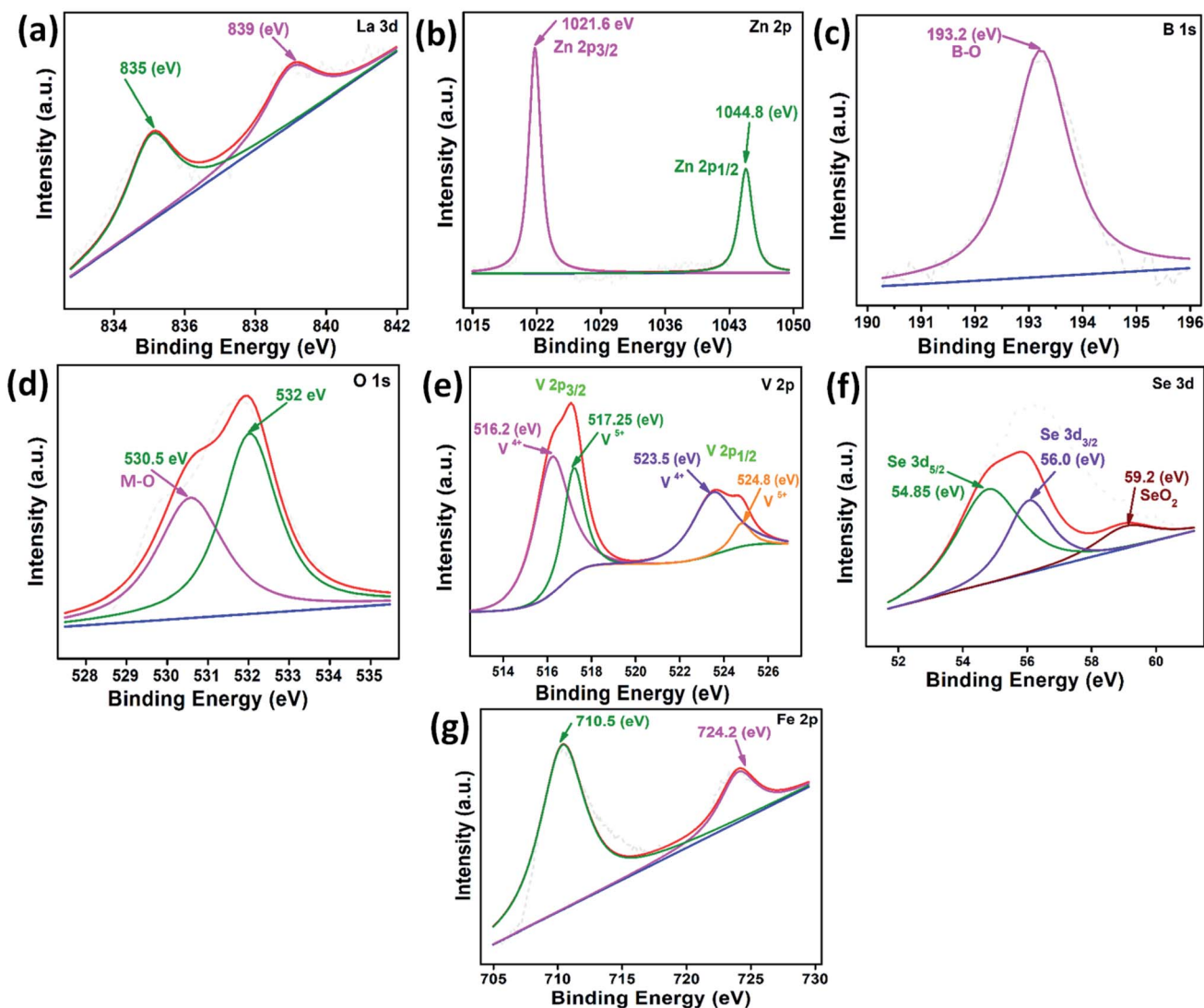


Fig. 9 Deconvoluted XPS of the tribofilm generated on the wear track in the presence of PO blended with LZB/VSe<sub>2</sub> after ASTM D4172 test (a) La 3d (b) Zn 2p (c) B 1s (d) O 1s (e) V 2p (f) Se 3d and (g) Fe 2p.

surfaces get seized, and the consequent load is considered the seizure load, signifying the load-carrying capacity of the additive. Physically, the tribofilm is devastated at seizure load, and the lubricant fails to sustain the load. As apparent from the data, the increase in seizure load of the additives follows their antiwear/antifriction efficiencies; VSe<sub>2</sub> (2040 N), ZB (2138 N), LZB (2327 N), and (3310 N). Thus, the outstanding load-bearing ability is ostensible for the LZB/VSe<sub>2</sub>. The porous structure of LZB in the LZB/VSe<sub>2</sub> accounts for such a high load-bearing ability.

**3.2.5. Frictional power loss.** The power loss (P) due to frictional force was evaluated for base lube in the presence and absence of the additives using eqn (1). The contents are furnished in (S13.2).

$$P = 0.221 \times 3.6 \times \mu \text{ MJ} \quad (1)$$

Where  $\mu$  = coefficient of friction.

As mentioned in Table 1, for PO alone, very high power consumption (0.0628 MJ) was observed, while there is a significant reduction in power consumption for its blends with various additives; 0.059 MJ for VSe<sub>2</sub>, 0.0375 MJ for ZB, 0.0330 MJ for the LZB and 0.0190 for LZB/VSe<sub>2</sub>. Thus, the reinforced structure has minimum power consumption or maximum energy saving.

### 3.3. Morphological characteristics of wear scar surface

After conducting the antiwear test ASTM D4172, the surface characterization carried out by AFM and SEM assisted in enlightening the morphology of the wear track. The SEM micrographs of the wear track lubricated with PO and its admixture with LZB/VSe<sub>2</sub> (0.15% w/v) are furnished in Fig. 7.

A furrowed surface due to dreadful scratches for plain PO can be seen in the SEM micrograph; nevertheless, the improved surface is undoubtedly observed in the case of admixtures. The



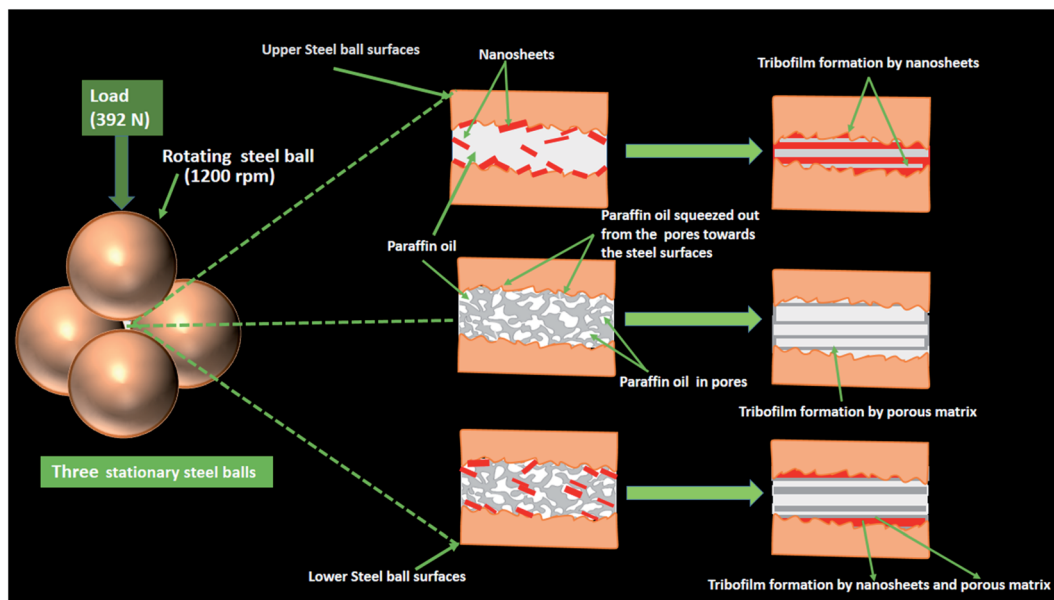


Fig. 10 The schematic diagram for the suggested mechanism of lubrication.

comparative degree of the surface evenness authenticates the results. The evenness of the surface can correlate very well with the MWD values provided in the inset of images. As anticipated, excellent smoothness of the surface is observed when admixture of the LZB/VSe<sub>2</sub> is applied for lubricity. Fig. 7f shows the EDX analysis of the wear track, confirming the presence of all elements of the additives, which demonstrates the actively adsorbed additive on the wear track. Boron, as an exception, is usually not identified because of its small size.<sup>6</sup> EDX spectra of the wear pathway of ZB, LZB, and VSe<sub>2</sub> are provided in ESI (Fig. S3†).

Furthermore, contact mode AFM was used for plain oil with and without additives to calculate the surface roughness of lubricated steel ball after performing the ASTM D4172 test. Fig. 8 describes the 3D and 2D AFM micrographs of the worn surfaces. The surface roughness values, area roughness (Sq), and line roughness (Rq) related to plain PO and its admixtures are provided in Fig. 8. Going from base oil to its admixtures, VSe<sub>2</sub>, ZB, LZB, and LZB/VSe<sub>2</sub>, there is a substantial decline in the Rq and Sq values. As expected, maximum smoothness and slightest roughness are perceived when LZB/VSe<sub>2</sub> is employed as a lubricant additive. Thus, the AFM results validated the evaluations based on SEM analyses. Additional roughness variables like Rm, Ra, Rp, Ry, Rv, Sa, Sy, Sp, Sm, and Sv, have been supplied in Table S1.†

#### 3.4. Characterization of tribofilm by XPS

After ASTM D4172 test, the XPS spectra of the worn surface in the presence of PO alone and blended with LZB/VSe<sub>2</sub> were recorded to examine the chemical states of the constituent elements of the tribofilm generated *in situ*. The deconvoluted core level spectra of La 3d, Zn 2p, B 1s, O 1s, V 2p, Se 3d, and Fe 2p are illustrated in Fig. 9, employing xps peak fit software.

The position of the peaks in XPS spectra of La 3d, Zn 2p, B 1s, O 1s, V 2p, and Se 3d shows that tribochemical oxidation has resulted in the formation of oxides of lanthanum (La<sub>2</sub>O<sub>3</sub>), zinc (ZnO), boron (B<sub>2</sub>O<sub>3</sub>), vanadium (V<sub>2</sub>O<sub>5</sub>) and selenium (SeO<sub>2</sub>). Moreover, the peaks that appear in the Fe 2p XPS spectrum at 710.5 eV (Fe 2p<sub>3/2</sub>) and 724.2 eV (Fe 2p<sub>1/2</sub>),<sup>12–17</sup> indicate the formation of Fe<sub>2</sub>O<sub>3</sub> through the oxidation of Fe of the steel.<sup>2,3,5,6</sup> Thus, the presence of various oxides, particularly ZnO,<sup>3</sup> La<sub>2</sub>O<sub>3</sub>,<sup>5</sup> B<sub>2</sub>O<sub>3</sub>,<sup>29</sup> and V<sub>2</sub>O<sub>5</sub>,<sup>52</sup> usually facilitate lubrication and promote the tribological properties of LZB/VSe<sub>2</sub>.

#### 3.5. Suggested mechanism of lubrication

The driving factor for tribological compatibility of the additives relies on their firmness to remain attached over the tribo-surfaces, eventually leading to tribofilm formation during tribological tests, which, in fact, supports the load. The composition, tenacity, and sustainability of the tribofilm are pivotal in understanding the observed efficacy of the additives.

The porous structure of LZB plays a crucial role in enhancing lubricating properties by acting as an intelligent oil reservoir that makes it a self-lubricating system to facilitate the pore structure for discharge of the base oil, which is already stored in pores to the contacting surfaces consistently.<sup>37,38</sup> Meanwhile, through capillary imbibition, it can reuse the additional base oil into the internal pores in between and afterward the work.<sup>38</sup> Thus, the self-lubricating porous LZB shows the benefits of high accuracy, high consistency, and enduring lubrication. Mesopores of LZB fill with only base lube, which is released when required, while the macropores severely affect the mechanical properties because of their merger with the neighbouring ones.<sup>40</sup> The macropores are also filled with some nanosheets, which are necessary for lower oil consumption. Thus, medium porosity is needed for better consistency of lubrication.<sup>38</sup> The doping of lanthanum has boosted lubrication due to defects. As



a consequence of defects, the electronic structure gets affected due to the formation of slip systems, and ultimately, shear strength is diminished.<sup>3</sup>

Undoubtedly, the layered structure of VSe<sub>2</sub> has facilitated the sliding motion due to weak van der Waals forces.<sup>3,5,6</sup> Under thermo-mechanical effects<sup>40</sup> of the tribological test, the nanosheets were squeezed and smeared on the worn surface of the porous LZB matrix due to high contact pressure. The drastic friction at the interface is therefore weakened. The outstanding tribological outcome of LZB/VSe<sub>2</sub> towards minimizing friction, wear, and increasing seizure load may be assigned to cooperative interaction amid the LZB and VSe<sub>2</sub> nanosheets,<sup>3,5,6</sup> as depicted in the diagrammatic representation of lubrication mechanism, Fig. 10. The tribofilm made up of Vse<sub>2</sub> nanosheets on the LZB matrix containing mostly self-lubricating oxides, ZnO, B<sub>2</sub>O<sub>3</sub>, La<sub>2</sub>O<sub>3</sub>, V<sub>2</sub>O<sub>5</sub> validates the suggested cooperative interaction.

## 4 Conclusions

Nanoporous zinc borate and, La-doped zinc borate were prepared using auto combustion route willfully to take advantage of porosity and doping in enhancing the triboactivity. Assessment of tribological activity by ASTM D4172 test and ASTM D5183 tests divulged the effect of porosity and lanthanum doping on the observed results. Hydrothermally prepared VSe<sub>2</sub> nanosheets were used for the furtherance of the tribological activity of LZB. The HR-SEM and TEM studies of LZB/VSe<sub>2</sub> revealed VSe<sub>2</sub> nanosheets physically adhered to LZB. The as-prepared nanomaterials were characterized by *p*-XRD, FT-IR, and XPS. Dispersion stability of the blends of nanomaterials in PO was studied by UV/visible spectroscopy. It was found that LZB/VSe<sub>2</sub> was the most stable even after 48 hours. The tribological data based on the tests mentioned above for the optimized concentration (0.15 %w/v) of the test materials manifest the highest antiwear and antifricition efficiencies of LZB/VSe<sub>2</sub> followed by LZB, ZB, and VSe<sub>2</sub>. SEM and AFM studies of the wear track corroborate the above result. Analysis of the wear pathway by XPS reveals that the tribofilm comprises oxides of La, Zn, V, Se, B, and Fe<sub>2</sub>O<sub>3</sub>. Doping of La in zinc borate produced defects, further advancing the lubricating properties. Unambiguously, cooperative interaction between LZB and VSe<sub>2</sub> nanosheets governed the commendable tribo-activity of LZB/VSe<sub>2</sub>, demonstrating its candidature as aspiring friction and wear modifier for various lubrication systems.

## Author contributions

A. K. S. has done the experimental work, analyzed the data and compiled the manuscript. N. S. and Kavita helped throughout the experimentation and interpretation of spectra. D. K. V. and B. K. have assisted in AFM and XPS analysis. K. D. M. has helped in editing the manuscript. R. B. R. has conceived the idea and supervised the whole work. All contributing authors have carefully read the final manuscript and approved it.

## Conflicts of interest

There is no conflict of interest.

## Acknowledgements

The authors A. K. Singh, N. Shukla, and D. K. Verma are thankful to the Head, Department of Chemistry, I. I. T. (BHU) Varanasi, India, for financial assistance as TAs. Kavita and B. K. are grateful to CSIR, New Delhi and UGC, New Delhi, respectively, for their SRF. The authors express a deep sense of gratitude to the Incharge, CIFIC, I. I. T. (BHU) Varanasi for providing TEM and SEM with EDX facilities and recording XPS spectra.

## References

- 1 D. K. Verma, N. Shukla, B. Kumar, A. K. Singh, K. Shahu, M. Yadav, K. Y. Rhee and R. B. Rastogi, *Nanomaterials*, 2020, **10**, 707–726.
- 2 A. K. Singh, A. Yadav, A. Indra and R. B. Rastogi, *Colloids Surf., A*, 2021, **613**, 126100.
- 3 A. K. Singh, N. Shukla, D. K. Verma, Kavita, B. Kumar and R. B. Rastogi, *Ind. Eng. Chem. Res.*, 2021, **60**, 864–874.
- 4 Y. Zhang, J. Yan, X. Ren, L. Pang, H. Chen and S. F. Liu, *Int. J. Hydrogen Energy*, 2017, **42**, 5472–5477.
- 5 N. Shukla, D. K. Verma, A. K. Singh, B. Kumar, Kavita and R. B. Rastogi, *ACS Appl. Nano Mater.*, 2020, **3**, 8012–8026.
- 6 D. K. Verma, J. Kuntail, B. Kumar, A. K. Singh, N. Shukla, Kavita, I. Sinha and R. B. Rastogi, *ACS Appl. Nano Mater.*, 2020, **3**, 5530–5541.
- 7 Y. Li, H. Lu, Q. Liu, L. Qin and G. Dong, *Tribol. Int.*, 2019, **137**, 22–29.
- 8 H. Lu, L. Chen, Q. Liu, Y. Li and L. Gao, *Mater. Chem. Phys.*, 2021, **272**, 125053.
- 9 K. Cao, C. Li, C. Yonghua, H. Tang, F. Yan, H. Song and X. Yang, *Tribol. Int.*, 2012, **55**, 297–301.
- 10 R. Qu, X. Wen, Y. Zhao, T. Wang, R. Yao and J. Lu, *Ultrason. Sonochem.*, 2021, **73**, 105491.
- 11 F. Zhang, J. Sun, Y. Lu, X. Feng, C. Li, J. Xu and G. G. Tang, *Mater. Res. Express*, 2019, **6**, 095058.
- 12 X. H. Zhang, M. Q. XUEb, Z. D. Huang, Z. P. Wang and F. Yang, *Chalcogenide Lett.*, 2015, **12**, 645–651.
- 13 Y. Zhao, H. Mei, P. Chang, Y. Yang, W. Huang, Y. Liu, L. Cheng and L. Zhang, *ACS Appl. Mater. Interfaces*, 2021, **13**, 34984–34995.
- 14 S. Domínguez-Meister, T. C. Rojas, M. Brizuela and J. C. Sánchez-López, *Sci. Technol. Adv. Mater.*, 2017, **18**, 122–133.
- 15 M. Q. Xue, Z. P. Wang, F. Yuan, G. S. Luo, X. H. Zhang, W. Wei, H. Tang and C. S. Li, *Chalcogenide Lett.*, 2017, **14**, 37–42.
- 16 X. Zhang, M. Xue, X. Yang, G. Luo and F. Yang, *Micro Nano Lett.*, 2015, **10**, 339–342.
- 17 Z. Chen, L. Guo, H. Yan, H. Yao, L. Li and Q. Liu, *Composites, Part B*, 2019, **161**, 263–271.
- 18 F. X. Zhang, Y. Q. Chu and C. S. Li, *Materials*, 2019, **12**, 1854.





- 19 J. Sun, G. Tang, C. Li, X. Ji, W. Liang and H. Tang, *Micro Nano Lett.*, 2013, **8**, 294–297.
- 20 W. Zhao, B. Dong, Z. Guo, G. Su, R. Gao, W. Wang and L. Cao, *ChemComm*, 2016, **52**, 9228–9231.
- 21 M. Yan, X. Pan, P. Wang, F. Chen, L. He, G. Jiang, J. Wang, J. Z. Liu, X. Xu, X. Liao and J. Yang, *Nano Lett.*, 2017, **17**, 4109–4115.
- 22 L. Li, L. Pang, Q. Zhao, W. Liu and Y. Su, *J. Mater. Chem. C*, 2020, **8**, 1104–1109.
- 23 F. Ming, H. Liang, Y. Lei, W. Zhang and H. N. Alshareef, *Nano Energy*, 2018, **53**, 11–16.
- 24 C. Yang, J. Feng, F. Lv, J. Zhou, C. Lin, K. Wang, Y. Zhang, Y. Yang, W. Wang, J. Li and S. Guo, *Adv. Mater.*, 2018, **30**, 1800036.
- 25 Y. Wang, B. Qian, H. Li, L. Liu, L. Chen and H. Jiang, *Mater. Lett.*, 2015, **141**, 35–38.
- 26 M. Narayanasamy, L. Hu, B. Kirubasankar, Z. Liu, S. Angaiah and C. Yan, *J. Alloys Compd.*, 2021, **882**, 160704.
- 27 T. G. Ulusoy Ghobadi, B. Patil, F. Karadas, A. K. Okyay and E. Yilmaz, *Acs Omega*, 2017, **2**, 8319–8329.
- 28 Y. Huang, S. Han, S. Liu, Y. Wang and J. Li, *Ind. Lubr. Tribol.*, 2014, **66**, 143–150.
- 29 G. Kecheng, C. Boshui, X. Ming, W. Jiu, F. Jianhua and W. Jiang, *China Pet. Process. Petrochem. Technol.*, 2016, **18**, 92–99.
- 30 Y. Tian, Y. Guo, M. Jiang, Y. Sheng, B. Hari, G. Zhang, Y. Jiang, B. Zhou, Y. Zhu and Z. Wang, *Mater. Lett.*, 2006, **60**, 2511–2515.
- 31 Y. Tian, W. Zhou, L. Yu, F. Meng, K. Yu, X. Ding, M. Li and Z. Wang, *Mater. Lett.*, 2007, **61**, 506–510.
- 32 C. Zhao, Y. Jiao, Y. K. Chen and G. Ren, *Tribol. Trans.*, 2014, **57**, 425–434.
- 33 C. Zhao, Y. K. Chen, Y. Jiao, A. Loya and G. G. Ren, *Tribol. Trans.*, 2014, **70**, 155–164.
- 34 P. R. Wu, Y. M. Feng, T. Ge, Y. C. Kong, Z. S. Ma, Z. Liu and Z. L. Cheng, *J. Ind. Eng. Chem.*, 2018, **63**, 157–167.
- 35 Z. L. Cheng, W. Li and Z. Liu, *J. Alloys Compd.*, 2017, **705**, 384–391.
- 36 J. X. Dong and Z. S. Hu, *Tribol. Int.*, 1998, **31**, 219–223.
- 37 J. Wang, H. Zhao, W. Huang and X. Wang, *Wear*, 2017, **380**, 52–58.
- 38 C. Wang, D. Zhang, Q. Wang, H. Ruan and T. Wang, *Tribol. Lett.*, 2020, **68**, 1–9.
- 39 Y. Lei, J. Du, X. Pang, H. Wang, H. Yang and J. Jiang, *Mater. Res. Express*, 2018, **5**, 056512.
- 40 G. Xiao, B. Zhao and W. Ding, *Int. J. Adv. Manuf. Syst.*, 2021, **114**, 397–405.
- 41 Z. Cheng, H. Gong, Z. Wang, L. Zhu and G. Xie, *Ceram. Int.*, 2022, **48**, 8031–8038.
- 42 K. Januchta, R. E. Youngman, L. R. Jensen and M. M. Smedskjaer, *J. Non Cryst. Solids*, 2019, **520**, 119461.
- 43 N. Kucuk, I. Kucuk, M. Cakir and S. K. Keles, *J. Lumin.*, 2013, **139**, 84–90.
- 44 N. Kucuk, A. H. Gozel, M. Yüksel, T. Dogan and M. Topaksu, *Appl. Radiat. Isot.*, 2015, **104**, 186–191.
- 45 D. K. Verma, B. Kumar, Kavita and R. B. Rastogi, *ACS Appl. Mater. Interfaces*, 2018, **11**, 2418–2430.
- 46 K. Xu, P. Chen, X. Li, C. Wu, Y. Guo, J. Zhao, X. Wu and Y. Xie, *Angew. Chem., Int. Ed.*, 2013, **125**, 10671–10675.
- 47 A. S. Kipeck, N. B. Acarali, E. M. Derun, N. Tugrul and S. Piskin, *Int. J. Mater. Metall. Eng.*, 2013, **7**, 285–289.
- 48 C. P. Gerlach and J. Arnold, *Inorg. Chem.*, 1996, **35**, 5770–5780.
- 49 A. Ghobadi, T. G. U. Ghobadi, A. K. Okyay and E. Ozbay, *Photonics Res.*, 2018, **6**, 244–253.
- 50 F. Spadaro, A. Rossi, E. Lainé, J. Hartley and N. D. Spencer, *Phys. Chem. Glasses: Eur. J. Glass Sci. Technol., Part B*, 2016, **57**, 233–244.
- 51 Y. M. Li, C. Deng, J. W. Long, S. C. Huang, Z. Y. Zhao and Y. Z. Wang, *Polym. Degrad. Stab.*, 2018, **153**, 325–332.
- 52 Kavita, A. K. Singh, N. Shukla, D. K. Verma, B. Kumar, S. Singh and R. B. Rastogi, *Colloids Surf., A*, 2022, **642**, 128644.

